Report

Neuron

Long-Range Guidance of Spinal Commissural Axons by Netrin1 and Sonic Hedgehog from Midline Floor Plate Cells

Graphical Abstract

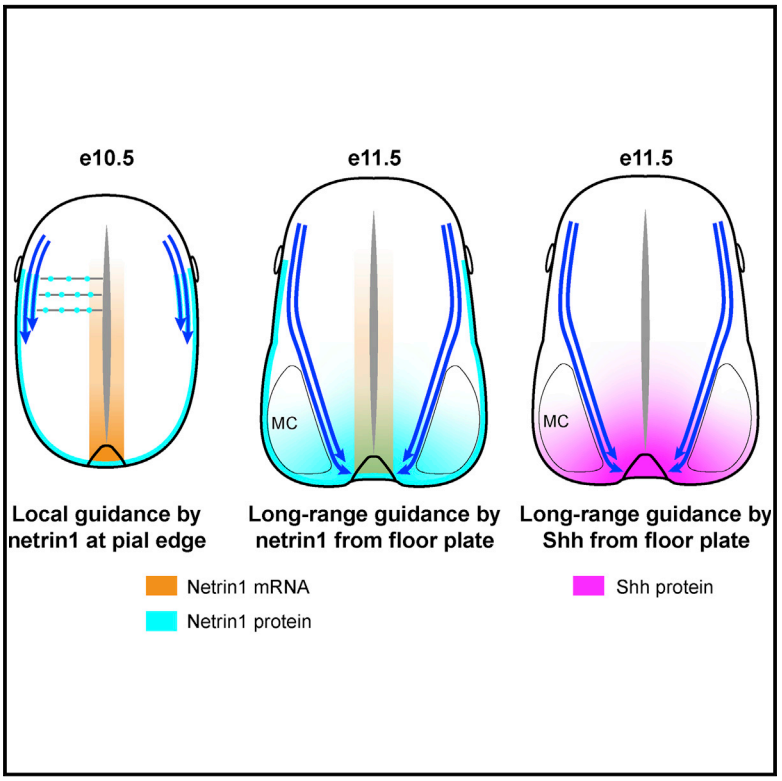

Authors

Zhuhao Wu, Shirin Makihara, Patricia T. Yam, ..., Alain Chédotal, Frédéric Charron, Marc Tessier-Lavigne

Correspondence

frederic.charron@ircm.qc.ca (F.C.), tessier3@stanford.edu (M.T.-L.)

In Brief

Recent studies have queried the role of netrin1 from floor plate (FP-netrin1) in guiding commissural axons. Wu et al. show that, in spinal cord, FP-netrin1 is required and acts at long range to guide commissural axons, collaborating with Shh.

Highlights

- Floor-plate-derived netrin1 (FP-netrin1) guides commissural axons at long range
- FP-netrin1 and Shh collaborate to guide commissural axons in the ventral spinal cord
- Both FP-netrin1 and ventricular zone-netrin1 contribute to commissural axon guidance
- FP-netrin1 may guide via haptotaxis and/or chemotaxis

Wu et al., 2019, Neuron *101*, 635–647
February 20, 2019
https://doi.org/10.1016/j.neuron.2018.12.025

CellPress

Neuron
Report

Long-Range Guidance of Spinal Commissural Axons by Netrin1 and Sonic Hedgehog from Midline Floor Plate Cells

Zhuhao Wu,[1,8] Shirin Makihara,[2,3,8] Patricia T. Yam,[2,8] Shaun Teo,[1,8] Nicolas Renier,[1,8] Nursen Balekoglu,[2,3] Juan Antonio Moreno-Bravo,[4] Olav Olsen,[1] Alain Chédotal,[4] Frédéric Charron,[2,3,5,6,9,*] and Marc Tessier-Lavigne[1,7,9,10,*]
[1]Laboratory of Brain Development and Repair, The Rockefeller University, New York, NY 10065, USA
[2]Montreal Clinical Research Institute (IRCM), 110 Pine Avenue West, Montreal, QC H2W 1R7, Canada
[3]Integrated Program in Neuroscience, McGill University, Montreal, QC H3A 2B4, Canada
[4]Sorbonne Université, INSERM, CNRS, Institut de la Vision, 17 Rue Moreau, 75012 Paris, France
[5]Division of Experimental Medicine, Department of Anatomy and Cell Biology, Department of Biology, McGill University, Montreal, QC H3A 2B2, Canada
[6]Department of Medicine, University of Montreal, Montreal, QC H3T 1J4, Canada
[7]Department of Biology, Stanford University, Stanford, CA 94305, USA
[8]These authors contributed equally
[9]Senior author
[10]Lead Contact
*Correspondence: frederic.charron@ircm.qc.ca (F.C.), tessier3@stanford.edu (M.T.-L.)
https://doi.org/10.1016/j.neuron.2018.12.025

SUMMARY

An important model for axon pathfinding is provided by guidance of embryonic commissural axons from dorsal spinal cord to ventral midline floor plate (FP). FP cells produce a chemoattractive activity, comprised largely of netrin1 (FP-netrin1) and Sonic hedgehog (Shh), that can attract the axons at a distance *in vitro*. *netrin1* is also produced by ventricular zone (VZ) progenitors along the axons' route (VZ-netrin1). Recent studies using region-specific *netrin1* deletion suggested that FP-netrin1 is dispensable and VZ-netrin1 sufficient for netrin guidance activity *in vivo*. We show that removing FP-netrin1 actually causes guidance defects in spinal cord consistent with long-range action (i.e., over hundreds of micrometers), and double mutant analysis supports that FP-netrin1 and Shh collaborate to attract at long range. We further provide evidence that netrin1 may guide via chemotaxis or haptotaxis. These results support the model that netrin1 signals at both short and long range to guide commissural axons in spinal cord.

INTRODUCTION

An important model for long-range axon pathfinding is provided by the stereotyped guidance of spinal commissural axons from their cell bodies in the dorsal spinal cord to FP cells at the ventral midline. These axons initially grow near the pial surface and then break away from the edge when they reach the developing motor column (MC) and reorient toward the midline FP, largely skirting the MC (Figure 1A). Two lines of evidence suggested that this midline-directed growth over the last few hundred micrometers results at least partly from action of a chemoattractant(s) secreted from FP. *In vitro*, FP cells both stimulate outgrowth of commissural axons from explants (Tessier-Lavigne et al., 1988) and attract them within explants over ~150–200 μm (Placzek et al., 1990). *In vivo*, genetic deletion of FP cells (in *Gli2*$^{-/-}$ mice) does not affect commissural axon growth in dorsal spinal cord (Matise et al., 1999) but results in more axons inappropriately entering the MC in ventral spinal cord (Charron et al., 2003).

Subsequent studies identified netrin1 and Shh as the major chemoattractants from FP. Netrins were purified based on their ability to mimic the outgrowth-promoting activity of FP (Serafini et al., 1994) and also possess the turning activity of FP (Kennedy et al., 1994). However, *in vitro* analysis of FP cells from *netrin1* mutant mice showed that, although netrin1 accounts for the outgrowth-promoting activity of FP cells, an additional chemoattractant(s) must collaborate with netrin1 in mediating long-range attraction (Serafini et al., 1996). A second attractant was identified as Shh, which possesses only attractive, not outgrowth-promoting, activity (Charron et al., 2003). *In vitro*, netrin1 and Shh are redundant attractants: blockade of either alone does not impair FP attraction, but blocking both largely abolishes it (Charron et al., 2003; residual turning activity may be due to vascular endothelial growth factor [VEGF]; Ruiz de Almodovar et al., 2011). *In vivo*, deletion of the Shh signal transducer *Smo* or receptor *Boc* partially mimicked FP deletion, as more axons inappropriately entered the MC (Charron et al., 2003; Okada et al., 2006). It was expected that removal of netrin1 from FP might also impair guidance and augment the effect of blocking Shh.

Initial tests of netrin1 function *in vivo* involved analysis of germline hypomorphic and null mutants, which displayed commissural axon guidance defects throughout the spinal cord (Bin

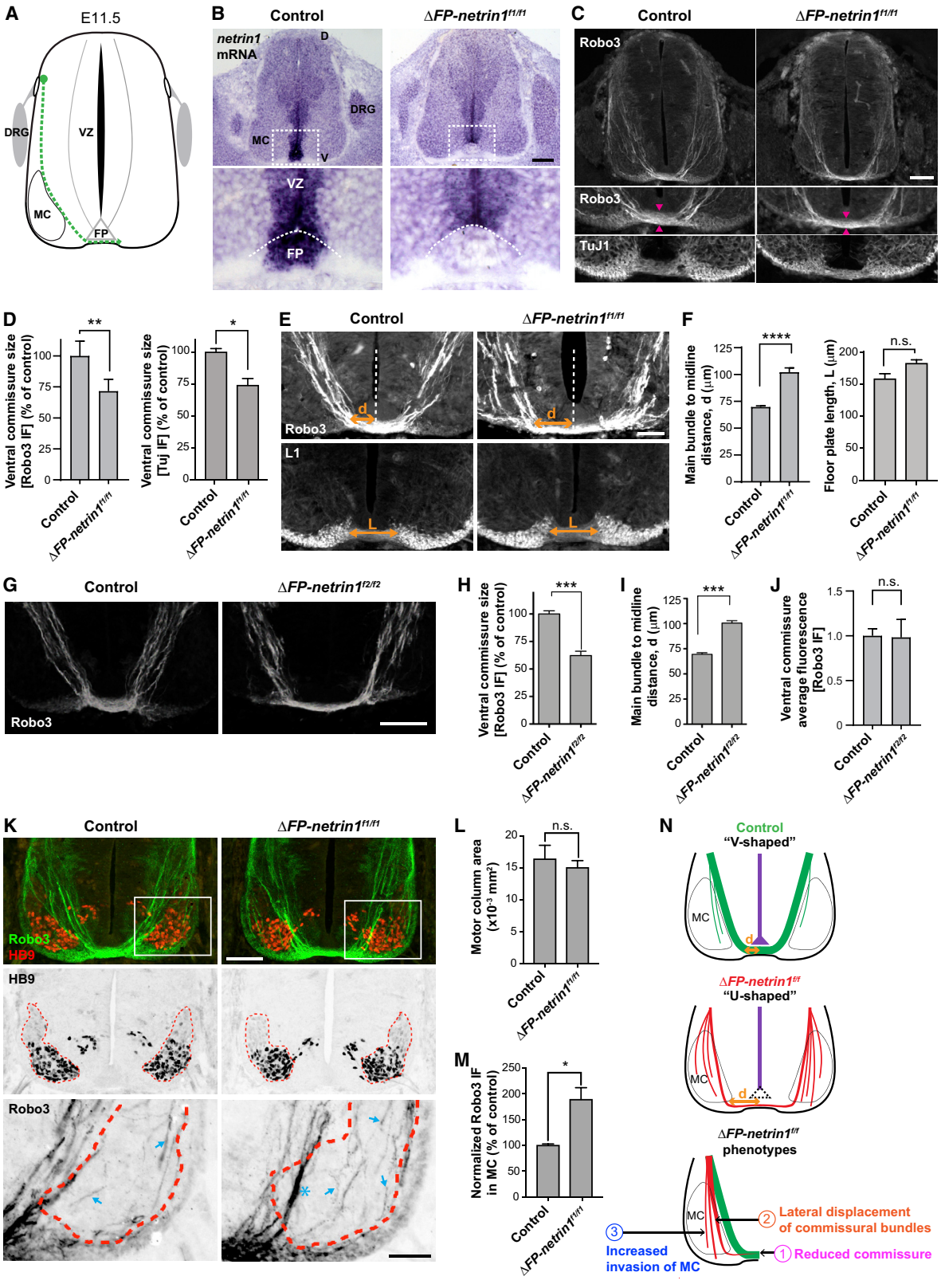

(legend on next page)

et al., 2015; Serafini et al., 1996; Yung et al., 2015) that are much more extensive than those seen with genetic deletion of just FP cells, reflecting that *netrin1* is produced not only by FP but also by progenitor cells in the ventricular zone (VZ) in the ventral two thirds of the spinal cord (Kennedy et al., 1994; Serafini et al., 1996). A role for *VZ-netrin1* was established by crossing the *Gli2*$^{-/-}$ mice (which lack FP so only possess *VZ-netrin1*) to a *netrin1* mutant (to remove both FP and *VZ-netrin1*), which resulted in more extensive misguidance than in *Gli2*$^{-/-}$ mice (Charron et al., 2003; Varadarajan et al., 2017). This showed that VZ-netrin1 contributes to guidance but did not define its precise role and left open the role of FP-netrin1.

The relative contributions of FP-netrin1 and VZ-netrin1 were recently studied more directly by selective deletion of *netrin1* in different regions of the spinal cord. Regional deletion of *VZ-netrin1* just in dorsal spinal cord produced guidance defects consistent with a significant role for VZ-netrin1 (Varadarajan et al., 2017). However, that study and another (Dominici et al., 2017) found that regional deletion of *FP-netrin1* did not prevent many spinal commissural axons from reaching the midline. A similar approach in hindbrain again showed a major role for VZ-netrin1 and that deletion of FP-netrin1 did not prevent many commissural axons from reaching the midline (Dominici et al., 2017; Yamauchi et al., 2017). In fact, detailed quantitative analysis in hindbrain failed to reveal any defects following FP-netrin1 deletion, suggesting that FP-netrin1 is dispensable and VZ-netrin1 is sufficient for guidance in that region (Dominici et al., 2017; Yamauchi et al., 2017). However, detailed analysis of trajectories in spinal cord after FP-netrin1 deletion was not reported.

Here, we analyze the contribution of FP-netrin1 to guidance in spinal cord. Consistent with those reports, deletion of *FP-netrin1* using two independent *netrin1* conditional alleles did not prevent many commissural axons from reaching the FP. However, in contrast to the hindbrain, in spinal cord, we found that the commissure size is significantly reduced. Commissural axons also exhibit guidance defects in ventral spinal cord consistent with FP-netrin1 acting over a distance. Similar results are described in an independent study (Moreno-Bravo et al., 2019). Furthermore, removal of both FP-netrin1 and the Shh receptor Boc results in additive guidance defects, supporting the model that FP-netrin1 and Shh collaborate in long-range guidance in ventral spinal cord (Charron et al., 2003). We also demonstrate directly that substrate-bound netrin1 can promote

Figure 1. Floor-Plate-Derived Netrin1 Acts at a Distance to Guide Commissural Axons in the Ventral Spinal Cord

(A) Illustration depicting the trajectory of commissural axons (green) as they project toward the floor plate (FP) in the spinal cord of an E11.5 mouse embryo. DRG, dorsal root ganglion; MC, motor column; VZ, ventricular zone.

(B) *netrin1 in situ* hybridization of E11.5 transverse spinal cord sections in *netrin1*$^{f1/f1}$ controls and *ShhCre;netrin1*$^{f1/f1}$ mutants, denoted as *ΔFP-netrin1*$^{f1/f1}$. Bottom panels show higher magnification of the FP region. The dotted line demarcates the FP-VZ boundary. D, dorsal; V, ventral; scale bar, 100 μm (top) or 25 μm (bottom).

(C) E11.5 transverse spinal cord sections of *netrin1*$^{f1/f1}$ control and *ΔFP-netrin1*$^{f1/f1}$ mouse embryos at the brachial level, stained for Robo3 (top). Higher magnification views of the FP region stained for Robo3 (middle) and TuJ1 (bottom) are also shown. The pair of magenta arrows denotes the thickness of the ventral commissure. Scale bar, 100 μm (top) or 50 μm (middle and bottom).

(D) Ratio of the ventral commissure thickness to the dorsoventral spinal cord length of E11.5 embryos, normalized to controls, measured using Robo3 (left) or Tuj1 (right). *netrin1*$^{f1/f1}$ controls (n = 6); *ΔFP-netrin1*$^{f1/f1}$ mutants (n = 6). **p = 0.0015 for Robo3+ axons, paired t test. At least 4 sections were measured for each embryo.

(E) Images of the ventral midline area of transverse spinal cord sections of E11.5 *netrin1*$^{f1/f1}$ control and *ΔFP-netrin1*$^{f1/f1}$ embryos, stained for Robo3 and L1. The distance "d" (orange arrows in top panels) from the main pre-crossing commissural axon bundle (as it arrives at the ventral edge) to the midline (dotted line) was measured. The floor plate length "L" (orange arrows in bottom panels) was measured as the distance between the post-crossing axon marker L1 in the two funiculi flanking the FP. Scale bar, 50 μm.

(F) The main bundle to midline distance d and floor plate length L of controls and *ΔFP-netrin1*$^{f1/f1}$ embryos were compared. For each embryo, at least 7 sections were measured. *netrin1*$^{f1/f1}$ controls (n = 6); *ΔFP-netrin1*$^{f1/f1}$ mutants (n = 6). ****p < 0.0001; not significant (ns), p = 0.578.

(G) The floor-plate region of E11.5 transverse spinal cord sections of control and *ΔFP-netrin1*$^{f2/f2}$ mouse embryos at the brachial spinal level, immunostained for Robo3. Scale bar, 100 μm.

(H) Ratio of the ventral commissure thickness to the dorsoventral spinal cord length of E11.5 embryos, normalized to controls, measured using Robo3. Controls (n = 22); *ΔFP-netrin1*$^{f2/f2}$ (n = 9). ***p < 0.001.

(I) Comparison of the main commissural axon bundle to midline d of controls (n = 22) and *ΔFP-netrin1*$^{f2/f2}$ embryos (n = 9). ***p < 0.001.

(J) Average Robo3 fluorescence in the ventral commissure, normalized to controls. Controls (n = 7); *ΔFP-netrin1*$^{f2/f2}$ (n = 4). ns, p = 0.93.

(K) Top: transverse spinal cord sections from E11.5 *netrin1*$^{f1/f1}$ control and *ΔFP-netrin1*$^{f1/f1}$ embryos co-immunostained for Robo3 (green) and HB9 (red). HB9 staining (middle) was used to define the MC (red dashed lines) for quantifying the Robo3+ axons invading this region (bottom). Scale bars, 100 μm (top and middle) and 30 μm (bottom).

(L) The MC area of controls (n = 3) and *ΔFP-netrin1*$^{f1/f1}$ embryos (n = 3) were compared. For each embryo, the areas of at least 7 sections were measured. ns, p = 0.603.

(M) To measure commissural axon invasion within the MC, the Robo3+ immunofluorescence intensity per unit area within the MC of controls (n = 3) and *ΔFP-netrin1*$^{f1/f1}$ embryos (n = 3) were normalized to controls and compared. For each embryo, the Robo3+ immunofluorescence intensity within the MC of at least 7 sections was measured. *p = 0.027.

(N) Model depicting the role of floor-plate-derived netrin1. Top: in the ventral spinal cord of control embryos, floor-plate (purple)-derived netrin1 acts at a distance and attracts commissural axons medially toward the ventral midline, preventing them from projecting into the MC. The commissural axon trajectory is typically "V-shaped" (green). Middle and bottom: in *ΔFP-netrin1*$^{f/f}$ mutants, the loss of floor plate netrin1 attraction results in (1) a reduced commissure thickness; (2) laterally displaced commissural axon bundles (red), resulting in a characteristic "U-shape"; and (3) increased commissural axon invasion into the MC. An overlay of the wild-type (green) and mutant (red) trajectories is shown for comparison (bottom).

For all graphs, error bars indicate SEM. All p values were derived from an unpaired t test, unless indicated otherwise.

See also Figure S1.

commissural axon outgrowth (apparently via a signaling, rather than an adhesive, mechanism) and that a gradient of soluble netrin1 is sufficient to direct commissural axon turning, suggesting that the long-range action of netrin1 could result from chemotaxis to soluble netrin and/or haptotaxis to substrate-bound netrin.

RESULTS

FP-Netrin1 Is Required for Correct Commissural Axon Guidance in the Ventral Spinal Cord

Like Varadarajan et al. (2017) and Dominici et al. (2017), we sought to evaluate the role of FP-netrin1 in commissural axon guidance by crossing a floxed *netrin1* allele (*netrin1*^{f1}) (Brunet et al., 2014) to a Shh-cre mouse line, which directs cre expression to FP. In *Shh*^{cre}*;netrin1*$^{f1/f1}$ embryos, *netrin1* transcripts are lost from FP cells, as assessed by *in situ* hybridization of spinal cord sections from embryonic day 11.5 (E11.5) embryos (Figure 1B), consistent with prior studies (Dominici et al., 2017; Varadarajan et al., 2017). As in those studies, we refer to these mice as *ΔFP-netrin1*$^{f1/f1}$. Of note, although *netrin1* transcripts are absent from FP, a high level of *netrin1* transcripts is observed immediately dorsal to FP (Figure 1B), consistent with the normal expression of *netrin1* within the VZ, which is highest just dorsal to the FP (Charron et al., 2003; Serafini et al., 1996). This could provide a residual source of netrin1 protein to guide axons ventrally in *ΔFP-netrin1* mutants.

Commissural axon trajectories were examined using an antibody to Robo3, which selectively labels commissural axons as they project to and across the FP (Sabatier et al., 2004). Consistent with prior studies (Dominici et al., 2017; Varadarajan et al., 2017), commissural axons still project ventrally and many reach the midline in *ΔFP-netrin1*$^{f1/f1}$ embryos (Figure 1C). However, close inspection shows defects at the midline as well as in axonal trajectories in the ventral spinal cord.

First, the thickness of the ventral commissure shows an ~30% reduction in mutants compared to controls (Figures 1C and 1D). The reduced thickness is also evident using antibodies to Tuj1 (Figures 1C and 1D), which labels all axons.

Second, the angle of projection through the ventral spinal cord is altered in *ΔFP-netrin1*$^{f1/f1}$ mutants. In control embryos, as commissural axons leave the pial edge, the main bundle of axons is oriented toward the ventral midline and intersects the ventral funiculus near the edge of the FP, providing a V-shaped appearance to the major bundles on both sides (Figures 1C and 1E). In *ΔFP-netrin1*$^{f1/f1}$ embryos, however, the main bundle projects more laterally, causing a U-shaped appearance (Figures 1C and 1E; see also Figures 1G, 1K, and 1N).

A quantitative measure of this alteration is provided by the distance "d" from the midline to the point of intersection of the main axon bundle with the ventral funiculus, which shows an ~45% increase in *ΔFP-netrin1*$^{f1/f1}$ embryos compared to controls (Figures 1E and 1F). In contrast to pre-crossing axons, post-crossing commissural axons in the ventral funiculus appear to have a normal placement with respect to the midline, as assessed with an antibody to L1 (Figures 1E and S1A), a marker upregulated by these axons after FP crossing. The distance "L" separating the two funiculi flanking the midline FP is unaltered in *ΔFP-netrin1*$^{f1/f1}$ embryos compared to controls (Figures 1E and 1F). A similar result is observed using antibodies to Robo1, another post-crossing axon marker (Figure S1B).

We repeated these experiments using a second conditional *netrin1* allele (Dominici et al., 2017), which we term *netrin1*^{f2}, and observed a similar reduction in commissure thickness and increase in d in *ΔFP-netrin1*$^{f2/f2}$ embryos (Figures 1G–1I). This provides independent confirmation that these defects result from removal of *netrin1* from the midline FP.

We considered the possibility that the reduction in ventral commissure thickness could result from the axons crossing the floor plate being squeezed into a tighter bundle, with a consequent increased axon density at the midline. We found that the ventral commissure had the same average Robo3 fluorescence intensity in *ΔFP-netrin1*$^{f2/f2}$ embryos compared to control embryos (Figure 1J), indicating that the reduction in commissure thickness results from fewer axons crossing the floor plate rather than a tighter bundle.

In addition to these two phenotypes, we found that *ΔFP-netrin1*$^{f1/f1}$ embryos have a greater number of axons invading the MC (visualized by labeling motoneurons with an antibody to HB9 [Figure 1K] or to Isl1/2 [Figure S1C]). In controls, some commissural axons normally break away from the main axon bundle and project toward the midline via the MC (Figure 1K, bottom left). In *ΔFP-netrin1* $^{f1/f1}$ embryos, however, more are seen taking this route (Figure 1K, bottom right), resulting in a doubling of Robo3+ immunofluorescence in the MC (Figure 1M), which itself does not change size (Figure 1L). A similar increased invasion of the MC is observed in *ΔFP-netrin1*$^{f2/f2}$ embryos (Figures S1C–S1E).

These three changes in *ΔFP-netrin1* mutants—reduced commissure thickness, lateral displacement of the main bundle, and increased invasion of the MC—are summarized in Figure 1N. The latter two are consistent with the model that netrin1 from FP attracts the axons at a distance toward the midline, so that in its absence the axons are less angled toward the FP and more prone to invading the MC. The reduced commissure thickness could reflect fewer axons reaching the midline and/or axons failing to cross the midline in a timely fashion after reaching it.

FP-Netrin1 and Shh Collaborate to Guide Commissural Axons in the Ventral Spinal Cord

Because FP-netrin1 and Shh were proposed to collaborate in attracting commissural axons, we next examined how defects present after deletion of *FP-netrin1* compare to those present after loss of Shh signaling and whether the effects are additive. Because Shh plays a role in patterning the ventral spinal cord, we disrupted Shh axon guidance using mice mutant in *Boc*, a Shh co-receptor required for Shh-mediated commissural axon guidance, but not spinal cord patterning (Okada et al., 2006). We generated littermates with three mutant genotypes: *ΔFP-netrin1*$^{f2/f2}$ single mutants; *Boc*$^{-/-}$ single mutants; and *ΔFP-netrin1*$^{f2/f2}$*; Boc*$^{-/-}$ double mutants. Using sections and whole-mount light sheet fluorescence microscopy, we found that all three mutant genotypes had defects in their Robo3+ commissural axon trajectories (Figures 2A and 2B; Video S1).

We first compared the single mutants. In contrast to *ΔFP-netrin1*$^{f2/f2}$ mutants, the commissure thickness and the midline

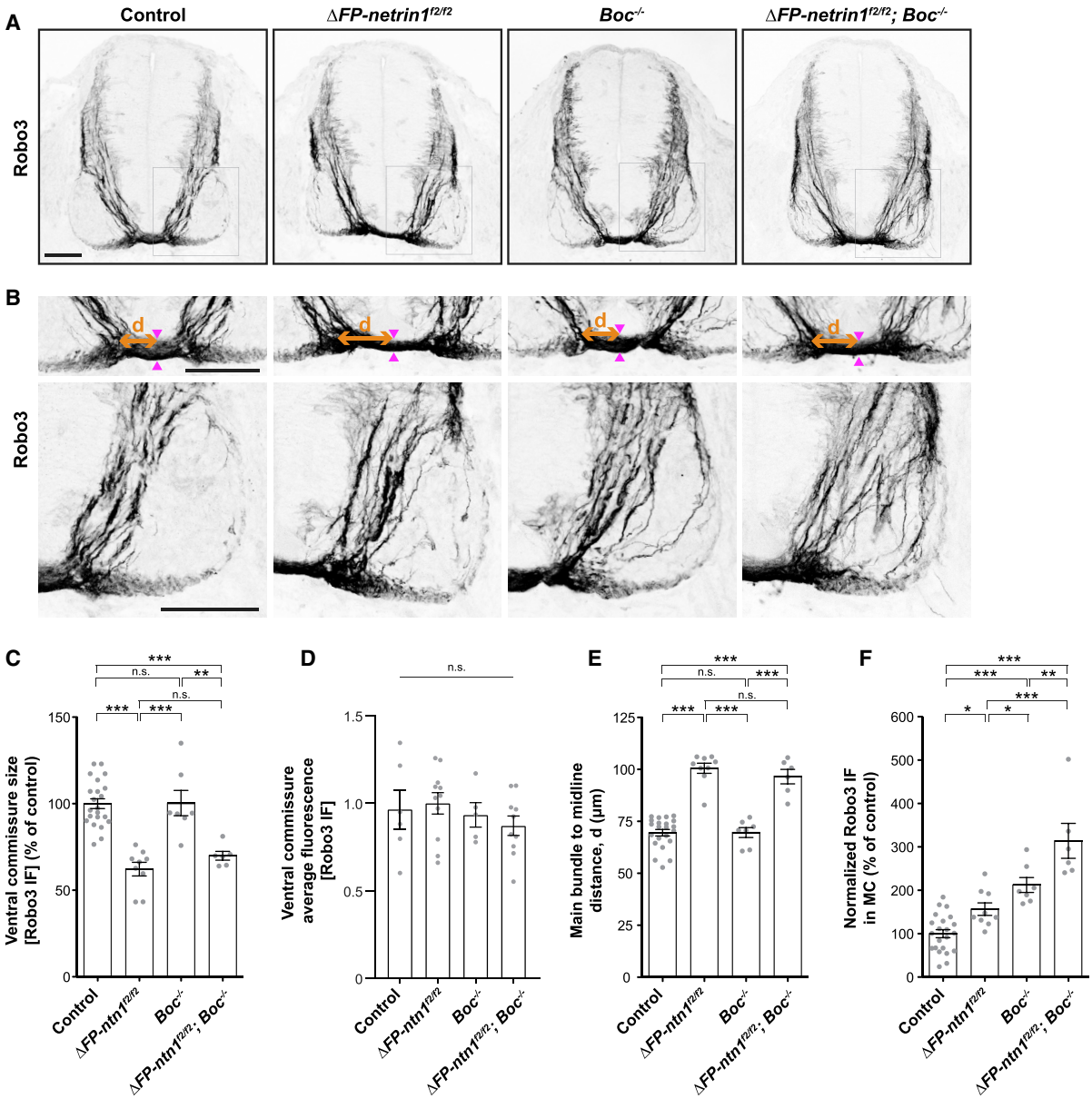

(legend on next page)

to main axon bundle distance in *Boc*$^{-/-}$ mutants were indistinguishable from controls (Figures 2C and 2E). However, like *ΔFP-netrin1*$^{f2/f2}$ mutants, *Boc*$^{-/-}$ mutants showed increased invasion of the MC compared to controls (Figure 2F) to an even greater extent than in *ΔFP-netrin1*$^{f2/f2}$ mutants.

We then compared the phenotype of the *ΔFP-netrin1*$^{f2/f2}$; *Boc*$^{-/-}$ mutants to the single mutants. Like the *ΔFP-netrin1*$^{f2/f2}$ single mutant, the double mutant had a reduced commissure thickness and increased midline to main axon bundle distance (Figures 2C and 2E). The reduced commissure thickness in the *ΔFP-netrin1*$^{f2/f2}$; *Boc*$^{-/-}$ mutants was not associated with a change in Robo3 fluorescence intensity (Figure 2D). Moreover, the single and double mutants did not have spinal cord patterning defects, as assessed by immunostaining for Pax6 and HNFβ (Figure S2).

Notably, the reduced commissure thickness (Figure 2C) and increased midline to main axon bundle distance (Figure 2E) were not more severe in the *FP-netrin1*$^{f2/f2}$; *Boc*$^{-/-}$ double mutant than in the *ΔFP-netrin1*$^{f2/f2}$ single mutant. In contrast, the *ΔFP-netrin1*$^{f2/f2}$; *Boc*$^{-/-}$ double mutants had a significantly greater MC invasion (Figure 2F) compared to each of the individual single mutants. In fact, the phenotype in the *ΔFP-netrin1*$^{f2/f2}$; *Boc*$^{-/-}$ double mutants appears to be an additive combination of the phenotypes seen in the single mutants (Figure 2G). Together, these results support the model that FP-derived netrin1 and Shh collaborate to guide commissural axons in the ventral spinal cord. Furthermore, the finding of defects in commissural axon trajectories more than 100 μm from the FP supports the model that both netrin1 and Shh guide commissural axons at long range.

Comparison to Guidance Defects in *netrin1*-null Animals

To provide additional context for the guidance role of FP-netrin1, we also reexamined guidance defects in *netrin1*-null mutants, which lack both FP-netrin1 and VZ-netrin1 and have multiple abnormalities in the trajectory of Robo3+ commissural axons (Figures 3A and S3A).

First, in the dorsal spinal cord, some axons are misrouted dorsally to the roof plate, those projecting ventrally parallel to the spinal cord edge are more disorganized than in wild-type and appear to pile up at the boundary with the ventral spinal cord, a few axons project medially into the ventricular zone, and some axons aberrantly project out of the dorsal roots. Second, in the ventral spinal cord, the characteristic bundles of axons projecting to the FP are absent, the axons are instead spread out over the region of the MC, a few axons aberrantly exit via the ventral roots, and the ventral commissure is almost completely absent (Figures 3A, 3B, and S3B; Videos S2 and S3).

Comparison of null and *ΔFP-netrin1* embryos reveals several points. First, the dorsal defects in the null mutant are not apparent in *ΔFP-netrin1* embryos, indicating that they require absence of VZ-netrin1. Second, the defects in the ventral spinal cord of *ΔFP-netrin1* embryos are much less extensive than in the null embryos, indicating that VZ-netrin1 also contributes with FP-netrin1 to ensuring proper guidance in the ventral spinal cord.

As well, although we saw a few Robo3+ axons projecting mediolaterally toward the ventricle in the null mutant, those projections were much less extensive than the dramatic medially directed projections reported in *netrin1* mutants when using neurofilament (NF) as a marker (Varadarajan et al., 2017), which we also see (Figures 3C and S3C–S3E). There is a particularly pronounced set of projections in the dorsal spinal cord at the level of the dorsal root entry zone (DREZ); similar extensive and dramatic medial projections at the level of the DREZ can be seen using TAG1, L1, TrkA, and TrkC as markers, but not Robo3 (Figures 3A, 3C, S3D, and S3E), indicating that these axons are likely sensory axons that have prematurely and aberrantly entered the spinal cord rather than commissural axons. In ventral spinal cord, a few additional NF+;Robo3− axons can be seen projecting more medially that do not appear to express the other markers (Figures 3C and S3C–S3E). They also do not appear to be aberrantly projecting motor axons (Figure S4). The identity of those axons remains uncertain.

Figure 2. Floor-Plate-Derived Netrin1 and Shh Collaborate to Guide Commissural Axons in the Ventral Spinal Cord

(A) E11.5 transverse spinal cord sections of control, *ΔFP-netrin1*$^{f2/f2}$, *Boc*$^{-/-}$, and *ΔFP-netrin1*$^{f2/f2}$; *Boc*$^{-/-}$ mouse embryos at the brachial spinal level, immunostained for Robo3. Scale bar, 100 μm.

(B) Enlargements of the floor plate region and the ventral spinal cord (boxed region in A). Magenta arrows denote the thickness of the ventral commissure. The main commissural axon bundle to midline distance d is indicated in orange. Scale bars, 100 μm.

(C) Ratio of the commissure thickness to the dorsoventral spinal cord length of E11.5 embryos, normalized to controls, measured using Robo3 immunofluorescence.

(D) Normalized average Robo3 fluorescence in the ventral commissure. p = 0.5440.

(E) Measurement of the main pre-crossing commissural bundle to midline d.

(F) Measurement of the Robo3 immunofluorescence intensity per unit area within the MC. Commissural neurons were immunostained for Robo3 and motor neurons for Isl1/2. Isl1/2 immunostaining was used to manually delineate the area of the MC (Figure S1C).

(C, E, and F) Each point represents an embryo (one section per embryo): control (n = 22 embryos); *ΔFP-netrin1*$^{f2/f2}$ (n = 9 embryos); *Boc*$^{-/-}$ (n = 7 embryos); and *ΔFP-netrin1*$^{f2/f2}$; *Boc*$^{-/-}$ (n = 6 embryos). Error bars indicate SEM. One-way ANOVA with Newman-Keuls multiple comparison test. *p < 0.05; **p < 0.01; ***p < 0.001.

(D) Each point represents an embryo (1–3 sections per embryo): control (n = 6 embryos); *ΔFP-netrin1*$^{f2/f2}$ (n = 11 embryos); *Boc*$^{-/-}$ (n = 5 embryos); and *ΔFP-netrin1*$^{f2/f2}$; *Boc*$^{-/-}$ (n = 10 embryos). Error bars indicate SEM. One-way ANOVA.

(G) Model depicting the role of FP-netrin1 and Shh in guiding commissural axons. In control embryos, FP-netrin1 and Shh act at a distance and attract commissural axons medially toward the ventral midline. In *ΔFP-netrin1*$^{f/f}$ mutants, the loss of FP-netrin1 results in (1) a reduced commissure thickness, (2) laterally displaced commissural axon bundles, and (3) increased commissural axon invasion into the MC. *Boc*$^{-/-}$ mutants have an unchanged commissure thickness and lateral positioning of commissural bundles. However, they have (3) increased invasion of commissural axons into the MC. *ΔFP-netrin1*$^{f/f}$; *Boc*$^{-/-}$ double mutants have an additive phenotype with (1) a reduced commissure thickness, (2) laterally displaced commissural axon bundles, and (3) even greater invasion of the MC. See also Figure S2 and Video S1.

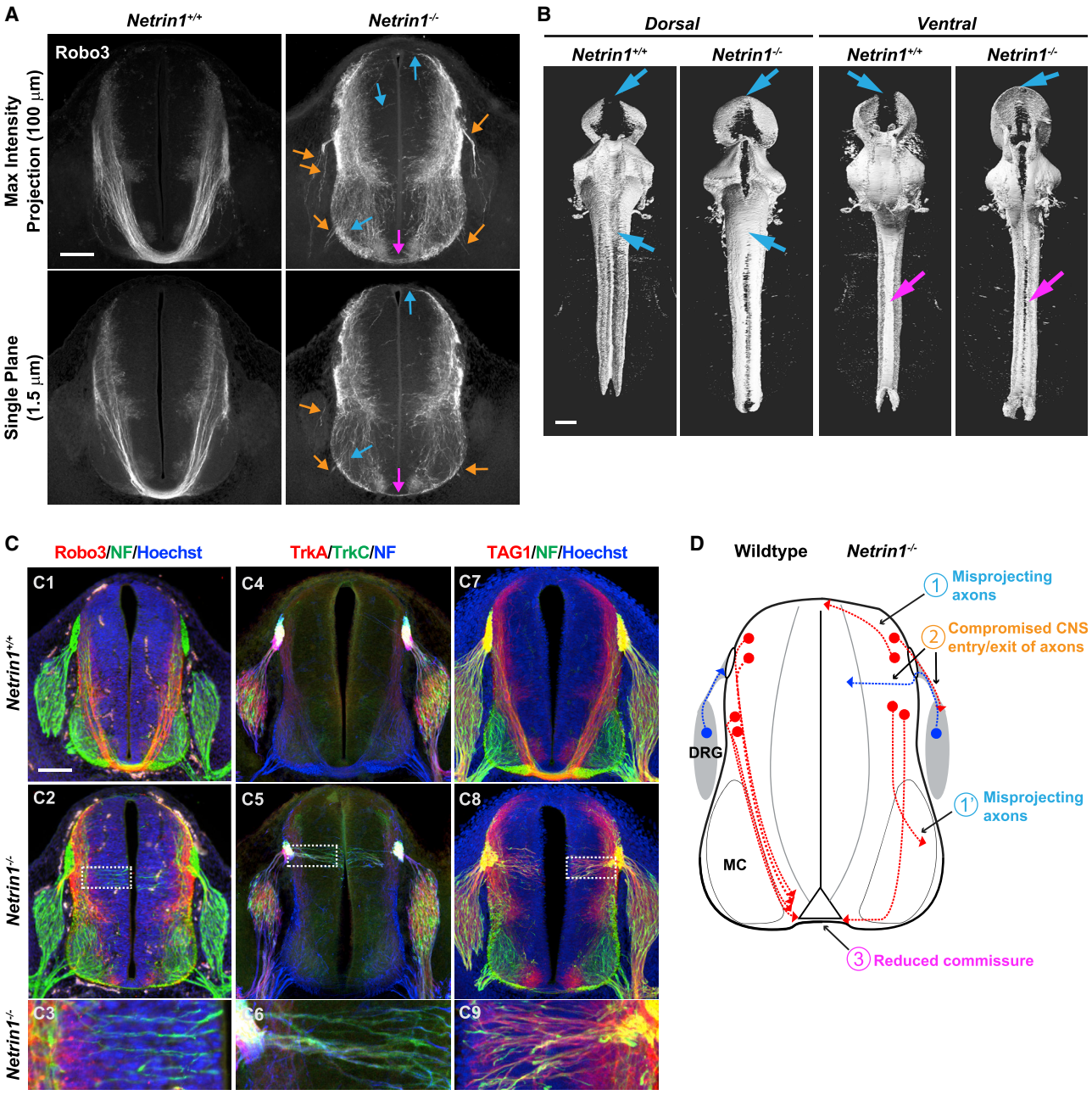

Figure 3. Loss of Netrin1 Causes Distinct Guidance Defects in Commissural and Sensory Axons

(A) Representative 100-μm maximum intensity projections and 1.5 μm (Z-step interval) single plane images of transverse spinal cord sections from E11.5 *netrin1*$^{+/+}$ and *netrin1*$^{-/-}$ embryos stained for Robo3. Colored arrows highlight commissural axons projecting toward and across the roof plate (blue) and exiting the CNS via the dorsal and ventral roots (orange) are shown, as well as wandering commissural axons (blue) and the reduced ventral commissure (magenta) are shown. Scale bar, 100 μm.

(B) Side-by-side surface projection images of cleared, whole-mount E11.5 *netrin1*$^{+/+}$ and *netrin1*$^{-/-}$ embryos stained for Robo3 viewed dorsally and ventrally. Blue arrows, dorsal midline, showing abnormal crossing in the mutant. Magenta arrows, ventral midline, showing reduced crossing in the mutant. Scale bar, 500 μm.

(C) Transverse spinal cord sections from E11.5 *netrin1*$^{+/+}$ and *netrin1*$^{-/-}$ littermate embryos stained for the following combinations of markers: (C1–C3) Robo3 (red), NF (green), and Hoechst (blue); (C4–C6) NF (blue) and the sensory axon markers TrkA (red) and TrkC (green); and (C7–C9) the more broadly expressed axonal markers TAG1 (red) and NF (green) as well as Hoechst (blue). Scale bar, 100 μm, 25 μm for higher magnifications.

(D) Schematic summarizing the major phenotypes observed in the spinal cord of *netrin1*$^{-/-}$ embryos (left half, wild-type; right half, mutant), including (1) misprojection of commissural axons within the spinal cord (red), including commissural axons projecting toward and across the roof plate (1) and commissural axons wandering in the ventral spinal cord (1'); (2) commissural axons exiting into the periphery via the dorsal and ventral roots (red) as well as premature CNS entry of sensory axons (blue); and (3) a reduced ventral commissure.

See also Figures S3 and S4 and Videos S2 and S3.

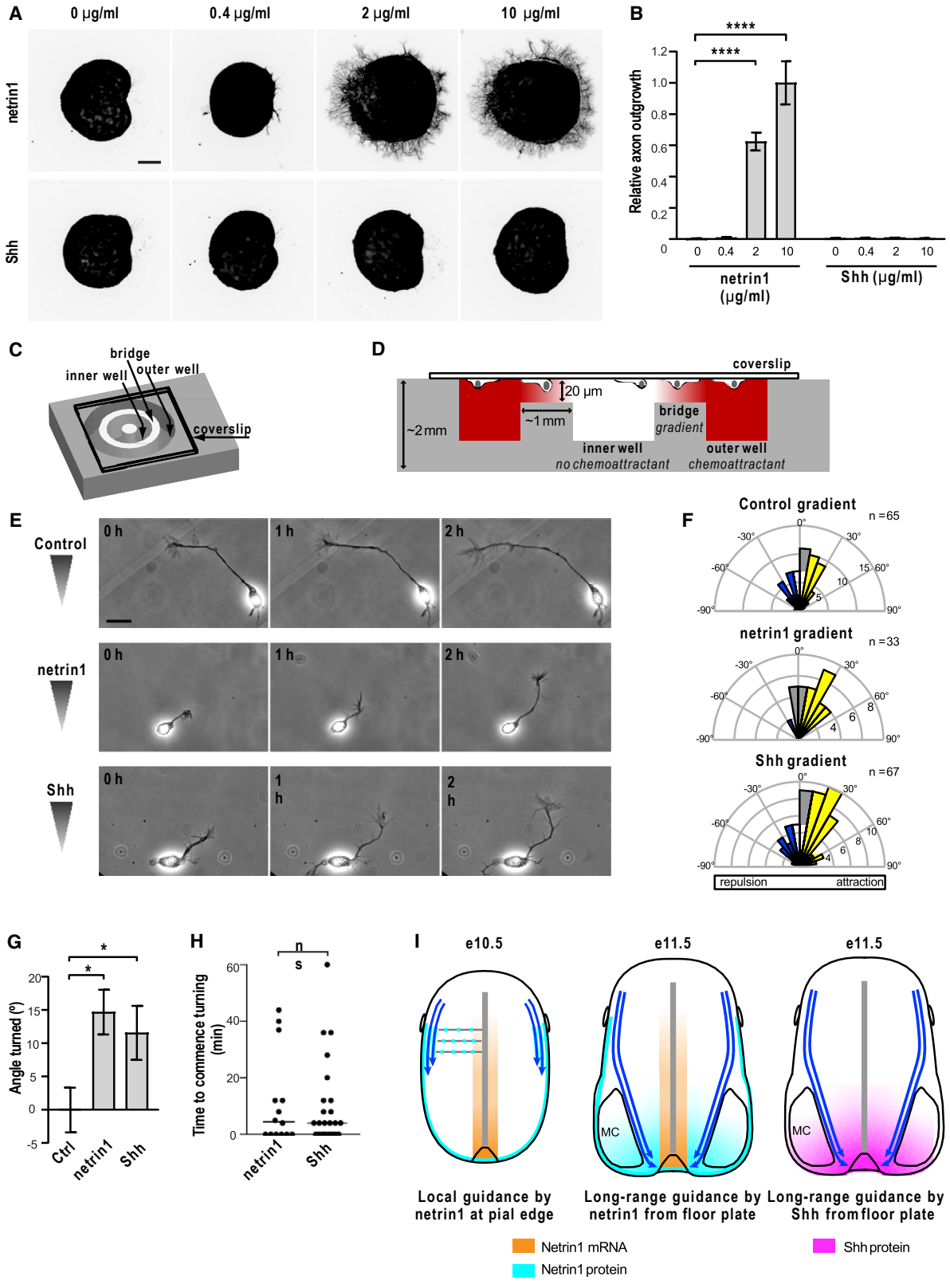

(legend on next page)

Netrin1 Directs Outgrowth and Growth Cone Turning of Commissural Axons

Our analysis of the *ΔFP-netrin1* mutants indicates that netrin1 acts at a distance to guide commissural axons *in vivo*. Netrins were initially purified as secreted and diffusible factors that also bind cell surfaces avidly (Serafini et al., 1994). Thus, the long-range action of netrin1 could result from soluble netrin1 inducing a chemotactic response or substrate-bound netrin1 inducing a haptotactic response (Kennedy et al., 1994).

To explore this, we first examined whether mouse commissural axons can grow on substrate-bound netrin1 and also examined responses to substrate-bound Shh. Culture surfaces were preincubated with 10 μg/mL poly-D-lysine (PDL) and then coated with netrin1 or Shh protein; after washing, explants of dorsal spinal cord from E11.5 mouse embryos were plated on these substrates. PDL alone did not support axon outgrowth, whereas netrin1 did in a dose-dependent fashion (Figures 4A and 4B). A similar dosage of Shh did not induce any outgrowth. Together, these results indicate that netrin1, but not Shh, can promote commissural axon outgrowth on a two-dimensional substrate. This netrin1-induced outgrowth appears independent of PDL-mediated adhesion, because netrin1 coating without PDL induced similar outgrowth (data not shown) whereas PDL coating alone did not induce outgrowth from explants across a broad range of concentrations (1, 2, 5, 10, 20, 50, 100, and 200 μg/mL; Figures 4A and 4B; data not shown)—even though PDL can support axon outgrowth from dissociated neurons (see below), which do not have a choice of substrate (unlike those in explants).

We next tested the effect of soluble netrin1 gradients on rat commissural axons, using an *in vitro* axon guidance assay based on the Dunn chamber (Figure 4C) that functions over short timescales (1 or 2 h) and directly measures growth cone turning (Yam et al., 2009). In this assay, dissociated dorsal spinal cord neurons are grown on PDL and then exposed to a chemoattractant gradient in the chamber (Figure 4D). To minimize possible substrate binding of the ligand, we used purified netrin1(VI-V)-Fc, a construct that retains the outgrowth-promoting activity of netrin1 (Keino-Masu et al., 1996) but binds surfaces less avidly than netrin1 (Mirzayan, 1997; Moore et al., 2012).

In a control gradient, axons grow with no change in their trajectory (Figure 4E; Video S4). In the presence of a netrin1(VI-V)-Fc or Shh gradient, the axons reorient up the gradient (Figure 4E; Videos S5 and S6). Quantification of the angle turned showed that there was no net turning of axons in a control gradient, whereas with netrin1 or Shh, there was significant turning up the gradient (Figures 4F and 4G), consistent with previous studies (Yam et al., 2009, 2012).

We also measured the turning latency of the axons. Because commissural axons grow episodically, with periods where the growth cone exhibits no net movement, we measured the time for an axon to begin reorienting toward the gradient after the start of axon growth. We found that the median time to begin turning up netrin1(VI-V)-Fc gradients was 4.5 min (Figure 4H), similar to that seen with Shh. For some axons, axon turning commenced at the same time as axon growth. Thus, soluble gradients of both netrin1(VI-V)-Fc and Shh can induce a rapid chemoattractive effect to direct turning of rodent commissural axons.

Taken together, our results provide direct evidence that substrate-bound netrin1, but not Shh, can stimulate outgrowth of rodent spinal commissural axons, whereas soluble gradients of either molecule can induce turning of these axons.

DISCUSSION

The guidance of spinal commissural axons to the FP has provided a valuable model for elucidating the logic and mechanisms of axon guidance. FP cells guide commissural axons at the midline through contact-dependent mechanisms but also secrete an outgrowth-promoting activity, mediated by netrin1, and a turning activity, mediated by both netrin1 and Shh, that can guide the axons over ~150–200 μm *in vitro*. Previous *in vivo* analysis supported a long-range guidance role for Shh but left open the role of FP-netrin1, if any, in guidance at a distance.

Using regional deletion of *netrin1* from FP, we reveal two defects in *ΔFP-netrin1* mutants that are consistent with a

Figure 4. Differential Effects of Netrin1 and Shh on Outgrowth versus Turning of Commissural Axons

(A) E11.5 mouse dorsal spinal cord explants were cultured for 16 h *in vitro* on glass slides preincubated with 10 μg/mL poly-D-lysine (PDL) and coated with varying netrin1 and Shh concentrations as indicated. Axon outgrowth was visualized by immunostaining for Tuj1. Scale bar, 100 μm.

(B) Quantification of axon outgrowth by measurement of Tuj1 fluorescence intensity, normalized to explant size. Two-way ANOVA with Sidak's multiple comparison test; ****$p < 0.0001$. Six explants per netrin condition and 4 explants per Shh condition are shown, from 3 independent experiments.

(C and D) Top (C) and side (D) view of a Dunn chamber, from Yam et al. (2009). A gradient forms over the annular bridge by diffusion of the chemoattractant from the outer to the inner well.

(E) Examples of growing commissural axons imaged in the Dunn chamber. All images have been rotated so that the gradient increases along the y axis. Scale bar, 20 μm.

(F) Commissural neurons were exposed to control, netrin1(VI-V-Fc), and Shh gradients. The distribution of angles turned by the commissural axons is represented by Rose histograms. Responses of individual neurons were clustered in 10° bins, and the number of neurons per bin is represented by the radius of each segment.

(G) The mean angle turned (±SEM) for commissural axons in control, netrin1(VI-V-Fc), and Shh gradients. One-way ANOVA with Dunnett's multiple comparisons test; *$p < 0.05$.

(H) Time for a growth cone to commence turning (after start of axon growth) in a netrin1(VI-V-Fc) or Shh gradient, for those axons which turned >20°; horizontal line is the median. Mann-Whitney test; $p = 0.7461$.

(I) Netrin1 protein is enriched along the pial edge in the dorsal spinal cord and found throughout the ventral spinal cord. Netrin is produced by cells in the ventral two thirds of the ventricular zone (VZ-netrin1), and by the FP (FP-netrin1). Netrin1 at the pial edge, which appears to derive primarily from VZ-netrin1, acts locally, and serves to confine commissural axons to the pial edge in the dorsal spinal cord (left). When axons enter the ventral spinal cord, they leave the pial edge and navigate around the MC to the midline. This guidance is directed by FP-netrin1 acting at a distance (middle), as well as by VZ-netrin1, which synergizes with FP-netrin1 in guidance in this region (not shown). In addition, Shh (also secreted by the FP) acts at a distance to guide commissural axons toward the FP (right). See also Videos S4, S5, and S6.

long-range role of FP-netrin1: a greater invasion of the MC and lateral displacement of the main commissural bundle. In addition, we observe thinning of the ventral commissure, which may reflect failure of some axons to reach and/or cross the midline in timely fashion. Identical defects were observed here using two distinct *netrin1* floxed alleles and in an independent study (Moreno-Bravo et al., 2019). Interestingly, only the first defect (greater invasion of the MC) was described in mice with conditional inactivation of *Smo* or germline inactivation of *Boc* (Charron et al., 2003; Okada et al., 2006; this study). Furthermore, the phenotypes in *ΔFP-netrin1; Boc* double mutants are essentially the sum of those in the single mutants.

Several conclusions can be drawn from this analysis.

First, the increased MC invasion in the mutants shows that FP-netrin1 and Shh both act on commissural axons at long range and supports the model (Charron et al., 2003) that both factors attract commissural axons over the last few hundred micrometers through ventral spinal cord (Figure 4I). An alternative, that loss of FP-netrin1 or Shh signaling causes some axons to defasciculate from the main bundle and to wander away, seems unlikely because loss of netrin1 *increases* fasciculation (Moreno-Bravo et al., 2019) and there is no evidence that Shh affects fasciculation. We also considered the possibility that FP-netrin1 or Shh normally mask a midline repellent activity, but this again seems unlikely because commissural axons become responsive to midline repellents only after midline crossing (Zou et al., 2000).

Second, the additivity of the *ΔFP-netrin1* and *Boc* ventral spinal cord invasion phenotypes supports the model that netrin1 and Shh from FP collaborate in guidance (Charron et al., 2003; Figure 4I). Interestingly, they appear fully redundant *in vitro* (Charron et al., 2003), but not *in vivo*, where deletion of either alone results in detectable phenotypes. The *in vivo* setting thus provides a more sensitive barometer than the *in vitro* assay for revealing their long-range guidance functions.

Third, the finding of two additional phenotypes in *ΔFP-netrin1* mutants compared to *Boc* mutants points to differences in the functions of netrin1 and Shh. What underlies these differences? One contributing factor could be that, whereas both netrin1 and Shh possess turning activity, only netrin1, not Shh, possesses outgrowth-promoting activity (Charron et al., 2003; this study). If the outgrowth-promoting activity helps make the midline environment permissive for growth, this could explain why, in absence of FP-netrin1, but not Shh, the commissure is reduced and main bundle displaced. The observation that the reduction in commissure thickness is transient, along with single axon tracing studies, suggest "stalling" of the axons as they approach the midline (Moreno-Bravo et al., 2019), which could reflect loss of a permissive action of FP-netrin1. A transient reduction in commissure thickness could also result, at least partly, from a delay in commissural axons reaching the midline when FP-netrin1 is absent, due to the slightly longer distance (~25 μm; Figure 1) to the midline caused by the U-shaped (compared to the V-shaped) trajectory.

Fourth, even in absence of both FP-netrin1 and Shh, many axons still reach the midline, indicating the operation of other collaborating guidance cues. Candidates include FP-derived VEGF, which is also attractive (Ruiz de Almodovar et al., 2011); the repellent NELL2, which may help guide the axons away from the MC (Jaworski et al., 2015); and VZ-netrin1 (see below).

Why have more than one FP-derived chemoattractant? We found that Shh and FP-netrin1 have additive, not redundant, effects on guidance *in vivo*. Thus, having two chemoattractants increases the fidelity of guidance; having a third, VEGF, may provide even greater fidelity.

Comparison with Prior Studies: A Difference between Spinal Cord and Hindbrain?

As mentioned, recent studies reported that many axons still reach the midline in spinal cord of *ΔFP-netrin1* mutants (Dominici et al., 2017; Varadarajan et al., 2017) but did not examine trajectories in detail in ventral spinal cord. The phenotypes we report (MC invasion, lateral bundle displacement, and commissure thinning) are robust, because we saw them with two different *netrin1* alleles and they were also seen by Moreno-Bravo et al. (2019); in fact, bundle displacement and commissure thinning can also be discerned in the micrographs of Varadarajan et al. (2017) (e.g., compare Figures 1R and 1Z). Further support for FP-netrin1 acting at a distance was provided by Moreno-Bravo et al. (2019), who, using single-axon tracing, showed errors on average 50 μm (and some 100 μm) away from FP in *ΔFP-netrin1* mutants and who observed that removing both *VZ-netrin1* and *FP-netrin1* has a synergistic effect in increasing MC invasion far from the midline. Collectively, these data support the proposed role of FP-netrin1 in long-range guidance.

In hindbrain, in contrast, extensive quantitative analysis of commissural axon trajectories in *ΔFP-netrin1* mutants failed to reveal obvious defects (Dominici et al., 2017; Yamauchi et al., 2017). Whether defects will result from also blocking Shh signaling remains to be determined, but the failure to detect defects in *ΔFP-netrin1* mutants in hindbrain contrasts with the observations in spinal cord.

What accounts for the apparent difference between hindbrain and spinal cord? The challenges facing commissural axons in these two regions are different. In spinal cord, after growing near the pial edge, the axons break away and dive toward the midline, largely avoiding the MC—perhaps because of the risk of exiting the spinal cord along with motor axons. The geometry of the hindbrain is different, however, as commissural axons grow near the pial edge over very long distances (millimeters) to the midline and do not break away as there is no MC to skirt, so it is less clear what contribution a chemoattractant acting over a few hundred micrometers would make to guidance.

These considerations suggest that long-range diffusible attractants, which appear to have a maximal range of ~150–250 μm when secreted from a single point, may be most useful when reorientation of axons is required within that distance of their target and when the geometry is appropriate—as is the case in spinal cord, but not hindbrain. In short, differences in the strategies needed for guidance may dictate when long-range attractants are useful to deploy and explain the difference between spinal cord and hindbrain.

Importance of VZ-Netrin1 and Role of Netrin1 in Guidance

Our results further support the importance of VZ-netrin1 in commissural axon guidance. Ever since the isolation of netrins (Serafini et al., 1994), it has been known that *netrin* transcripts

are present not just in FP (*netrin1*) but also in the ventral two-thirds of the spinal cord (a role played by *netrin2* in chick [Kennedy et al., 1994] and *netrin1* itself in mouse [Serafini et al., 1996]). It was proposed that FP-netrin1 serves "primarily to direct the last leg of commissural axon trajectories," with VZ-netrin1 contributing more extensively in other regions (Serafini et al., 1996). Involvement of VZ-netrin1 was supported by analysis of *Gli2*$^{-/-}$;*netrin1*$^{-/-}$ mice (Charron et al., 2003; Varadarajan et al., 2017) and evaluated more directly in regional deletion studies (Dominici et al., 2017; Varadarajan et al., 2017; Moreno-Bravo et al., 2019), which showed that removing VZ-netrin1 affects guidance in both dorsal and ventral spinal cord and synergizes with removal of FP-netrin1 in causing invasion of the MC. Our results fit with those studies, as we observe that defects in *ΔFP-netrin1* mutants are much more restricted than in germline *netrin1* mutants, which lack both *FP-netrin1* and *VZ-netrin1*. Of note, the high, graded level of *netrin1* transcripts in VZ just dorsal to the FP in *ΔFP-netrin1* mutants (Figure 1B) could provide a source of netrin1 protein that helps steer axons to the midline.

We also re-evaluated the trajectory of *netrin1*-null mutants through analysis of single optical sections and maximal projection of multiple sections, using the Robo3 marker at a resolution permitting visualization of individual axons (Figure 3). This analysis confirmed many phenotypes described previously (Bin et al., 2015; Laumonnerie et al., 2014; Serafini et al., 1996; Varadarajan et al., 2017; Varadarajan and Butler, 2017; Yung et al., 2015) but also underscored features that bear on the mechanism of guidance by netrin1. First, in ventral spinal cord, the axons cover much of the MC and do not show strong directionality toward the midline, consistent with netrin1 providing a directional cue. Second, in dorsal spinal cord, some axons project aberrantly toward the dorsal midline and the others are less well confined to the vicinity of the pial surface, fitting with the model that a corridor of netrin1 protein near the subpial surface (Kennedy et al., 2006; Varadarajan et al., 2017; Varadarajan and Butler, 2017) helps to confine and guide the axons in that region. Third, although a significant number of NF+ axons enter the VZ in the *netrin1* mutant (Varadarajan et al., 2017; Varadarajan and Butler, 2017), most are sensory and other axons (Masuda et al., 2008; Watanabe et al., 2006; this study) and invasion of the VZ by commissural axons is not a dominant phenotype.

Collectively, this analysis supports the model that netrin1 protein, enriched along the pial edge in dorsal spinal cord and found throughout ventral spinal cord (Kennedy et al., 2006; Varadarajan et al., 2017; Varadarajan and Butler, 2017), serves both to confine and to guide the axons—the latter perhaps by virtue of its graded distribution (Kennedy et al., 2006; Figure 4I).

Long- and Short-Range Actions, Chemotaxis, and Haptotaxis

Because FP cells can guide at a distance *in vitro*, initial studies of netrin1 focused on its potential long-range actions (Kennedy et al., 1994). However, netrins were purified as heparin-binding factors that partition between the soluble and the cell surface/extracellular matrix (ECM) fractions (Serafini et al., 1994). This raised the question "whether commissural axons detect the netrins in solution (a chemotactic response) or bound to cells or the ECM (a haptotactic response)," and raised the possibilities that their "range of diffusion … may be limited in the embryo" by substrate binding and that they may also have "contact-dependent guidance functions" (Kennedy et al., 1994). A short-range guidance function was demonstrated soon thereafter for retinal axons at the optic disc, where netrin1 protein remains localized to cells that produce it (Deiner et al., 1997), and later described in *Drosophila* as well (Akin and Zipursky, 2016; Brankatschk and Dickson, 2006; Timofeev et al., 2012).

In the spinal cord, netrin1 protein is enriched along the subpial edge in dorsal spinal cord and along the path of the axons in ventral spinal cord (Kennedy et al., 2006; MacLennan et al., 1997; Varadarajan et al., 2017; Varadarajan and Butler, 2017). Two lines of evidence suggest that VZ-netrin does not travel far (if at all) from its sites of production: in St. 17 chick embryos, where *netrin2* accounts for all *VZ-netrin* (Kennedy et al., 1994, 2006; Wang et al., 1999), netrin2-specific antibodies reveal that the dorso-ventral extent of netrin2 protein corresponds closely with that of *netrin2* transcripts (Kennedy et al., 2006), and in mouse, the dorsal-most extent of netrin1 protein expression similarly corresponds with that of *VZ-netrin1* expression (Varadarajan et al., 2017; Varadarajan and Butler, 2017). If so, VZ-netrin1 would presumably remain substrate bound and therefore guide via haptotaxis (Varadarajan et al., 2017), as also proposed in the hindbrain (Dominici et al., 2017); our finding that substrate-bound netrin1 can support mouse commissural axon outgrowth from explants supports this potential role. Because we found that the adhesive molecule PDL does not promote outgrowth from explants, the haptotactic response to netrin1 likely does not reflect simple adhesion *per se* and instead presumably reflects a signaling action.

What about FP-netrin1? In St. 17 chick embryos, where *netrin1* transcripts are only expressed in FP (Kennedy et al., 1994, 2006; Wang et al., 1999), netrin1-specific antibodies show that netrin1 protein is found a few hundred micrometers from FP (Kennedy et al., 2006), consistent with the distance over which netrin1 acts *in vitro* and the distance over which we detect guidance defects *in vivo* in *ΔFP-netrin1* mutants. It is therefore reasonable to assume that FP-netrin1 diffuses over that range to influence the axons. We cannot distinguish whether the axons detect FP-netrin1 in solution (chemotaxis) or after it binds to the substrate (haptotaxis), but the finding that rodent commissural axons can rapidly turn up a gradient of soluble netrin1 means that chemotaxis remains a possibility.

These considerations also suggest that FP-netrin1 may be more diffusible than VZ-netrin1 (or VZ-netrin2), fitting with the observation that explants of rat dorsal or ventral spinal cord, despite expressing *VZ-netrin1*, possess little to none of the long-range *in vitro* outgrowth-promoting and turning activities of FP explants (Placzek et al., 1990; Tessier-Lavigne et al., 1988). One possibility is that FP cells simply produce much more netrin protein than does the VZ, enabling an effect at a greater distance. Alternatively, VZ-netrin1 (or VZ-netrin2) may be less diffusible than FP-netrin1, either because of intrinsic differences in the proteins (e.g., posttranslational modifications) or, as recently suggested (Varadarajan et al., 2017), if there are differences in secretion mechanisms by VZ and FP cells, e.g., localized secretion and/or capture by endfeet of the radial progenitors that express *VZ-netrin1/2*.

Conclusions

Our study supports the classical model that commissural axons are guided at long range, i.e., over the last few hundred micrometers of their trajectory, by combined actions of netrin1 and Shh secreted by FP cells. These actions occur on top of an essential guidance role for VZ-netrin1, which appears to act more locally, as well as of other guidance cues. Our results also support the model that netrin1 guides commissural axons by confining and guiding them, perhaps through its graded distribution. More generally, our findings illustrate how the combined actions of long- and short-range guidance effects contribute to ensuring accurate guidance during development of axonal projections.

STAR★METHODS

Detailed methods are provided in the online version of this paper and include the following:

- KEY RESOURCES TABLE
- CONTACT FOR REAGENT AND RESOURCE SHARING
- EXPERIMENTAL MODEL AND SUBJECT DETAILS
  - Animals
- METHOD DETAILS
  - Section staining and microscopy
  - Whole embryo immunostaining and microscopy
  - Dorsal spinal cord (DSC) explant culture and outgrowth quantification on 2D substrates
  - Dissociated commissural neuron culture
  - Dunn chamber axon guidance assay and analysis
- QUANTIFICATION AND STATISTICAL ANALYSIS

SUPPLEMENTAL INFORMATION

Supplemental Information includes four figures and six videos and can be found with this article online at https://doi.org/10.1016/j.neuron.2018.12.025.

ACKNOWLEDGMENTS

We thank F. Depault, J. Ferent, J. Cardin, J. Barthe, and S. Ji for expert assistance, and T. Kennedy and S. Butler for helpful discussions. The 39.4D5 antibody was obtained from the Developmental Studies Hybridoma Bank developed under the auspices of the NICHD and maintained by The University of Iowa. Z.W. was supported by the Kavli Neural Systems Institute at The Rockefeller University. S.M. was supported by a Keidanren Ishizaka Memorial Foundation fellowship. S.T. was supported by fellowship funds from the Agency for Science, Technology and Research, Singapore (A*STAR). N.R. was supported by a post-doctoral fellowship from the Shelby White – Leon Levy Foundation. Work performed in the M.T.-L. laboratory was supported by The Rockefeller University and Stanford University, work performed in the A.C. laboratory was supported by a grant from the Agence Nationale de la Recherche (ANR-14-CE13-0004-01), and work performed in the F.C. laboratory was supported by the Canadian Institutes of Health Research (CIHR FDN334023), the Fonds de Recherche du Québec - Santé (FRQS), and the Canada Foundation for Innovation (CFI 33768). F.C. holds the Canada Research Chair in Developmental Neurobiology.

AUTHOR CONTRIBUTIONS

Z.W., S.M., P.T.Y., S.T., N.R., O.O., A.C., F.C., and M.T.-L. designed research; Z.W., S.M., P.T.Y., S.T., N.R., N.B., and J.A.M.-B. performed research; Z.W., S.M., P.T.Y., S.T., N.R., O.O., F.C., and M.T.-L. analyzed data; and A.C. contributed reagents. Z.W., P.T.Y., F.C., and M.T.-L. wrote the manuscript, with input and editing by the other authors.

DECLARATION OF INTERESTS

The authors declare no competing interests.

Received: July 10, 2018
Revised: November 15, 2018
Accepted: December 18, 2018
Published: January 17, 2019

REFERENCES

Akin, O., and Zipursky, S.L. (2016). Frazzled promotes growth cone attachment at the source of a Netrin gradient in the *Drosophila* visual system. eLife *5*, e20762.

Bin, J.M., Han, D., Lai Wing Sun, K., Croteau, L.P., Dumontier, E., Cloutier, J.F., Kania, A., and Kennedy, T.E. (2015). Complete loss of netrin-1 results in embryonic lethality and severe axon guidance defects without increased neural cell death. Cell Rep. *12*, 1099–1106.

Brankatschk, M., and Dickson, B.J. (2006). Netrins guide Drosophila commissural axons at short range. Nat. Neurosci. *9*, 188–194.

Brunet, I., Gordon, E., Han, J., Cristofaro, B., Broqueres-You, D., Liu, C., Bouvrée, K., Zhang, J., del Toro, R., Mathivet, T., et al. (2014). Netrin-1 controls sympathetic arterial innervation. J. Clin. Invest. *124*, 3230–3240.

Charron, F., Stein, E., Jeong, J., McMahon, A.P., and Tessier-Lavigne, M. (2003). The morphogen sonic hedgehog is an axonal chemoattractant that collaborates with netrin-1 in midline axon guidance. Cell *113*, 11–23.

Chi, J., Wu, Z., Choi, C.H.J., Nguyen, L., Tegegne, S., Ackerman, S.E., Crane, A., Marchildon, F., Tessier-Lavigne, M., and Cohen, P. (2018). Three-dimensional adipose tissue imaging reveals regional variation in beige fat biogenesis and PRDM16-dependent sympathetic neurite density. Cell Metab. *27*, 226–236.e3.

Deiner, M.S., Kennedy, T.E., Fazeli, A., Serafini, T., Tessier-Lavigne, M., and Sretavan, D.W. (1997). Netrin-1 and DCC mediate axon guidance locally at the optic disc: loss of function leads to optic nerve hypoplasia. Neuron *19*, 575–589.

Dominici, C., Moreno-Bravo, J.A., Puiggros, S.R., Rappeneau, Q., Rama, N., Vieugue, P., Bernet, A., Mehlen, P., and Chédotal, A. (2017). Floor-plate-derived netrin-1 is dispensable for commissural axon guidance. Nature *545*, 350–354.

Harfe, B.D., Scherz, P.J., Nissim, S., Tian, H., McMahon, A.P., and Tabin, C.J. (2004). Evidence for an expansion-based temporal Shh gradient in specifying vertebrate digit identities. Cell *118*, 517–528.

Jaworski, A., Tom, I., Tong, R.K., Gildea, H.K., Koch, A.W., Gonzalez, L.C., and Tessier-Lavigne, M. (2015). Operational redundancy in axon guidance through the multifunctional receptor Robo3 and its ligand NELL2. Science *350*, 961–965.

Keino-Masu, K., Masu, M., Hinck, L., Leonardo, E.D., Chan, S.S.-Y., Culotti, J.G., and Tessier-Lavigne, M. (1996). Deleted in Colorectal Cancer (DCC) encodes a netrin receptor. Cell *87*, 175–185.

Kennedy, T.E., Serafini, T., de la Torre, J.R., and Tessier-Lavigne, M. (1994). Netrins are diffusible chemotropic factors for commissural axons in the embryonic spinal cord. Cell *78*, 425–435.

Kennedy, T.E., Wang, H., Marshall, W., and Tessier-Lavigne, M. (2006). Axon guidance by diffusible chemoattractants: a gradient of netrin protein in the developing spinal cord. J. Neurosci. *26*, 8866–8874.

Langlois, S.D., Morin, S., Yam, P.T., and Charron, F. (2010). Dissection and culture of commissural neurons from embryonic spinal cord. J. Vis. Exp. 1773.

Laumonnerie, C., Da Silva, R.V., Kania, A., and Wilson, S.I. (2014). Netrin 1 and Dcc signalling are required for confinement of central axons within the central nervous system. Development *141*, 594–603.

Marillat, V., Cases, O., Nguyen-Ba-Charvet, K.T., Tessier-Lavigne, M., Sotelo, C., and Chédotal, A. (2002). Spatiotemporal expression patterns of slit and robo genes in the rat brain. J. Comp. Neurol. *442*, 130–155.

MacLennan, A.J., McLaurin, D.L., Marks, L., Vinson, E.N., Pfeifer, M., Szulc, S.V., Heaton, M.B., and Lee, N. (1997). Immunohistochemical localization of netrin-1 in the embryonic chick nervous system. J. Neurosci. *17*, 5466–5479.

Masuda, T., Watanabe, K., Sakuma, C., Ikenaka, K., Ono, K., and Yaginuma, H. (2008). Netrin-1 acts as a repulsive guidance cue for sensory axonal projections toward the spinal cord. J. Neurosci. *28*, 10380–10385.

Matise, M.P., Lustig, M., Sakurai, T., Grumet, M., and Joyner, A.L. (1999). Ventral midline cells are required for the local control of commissural axon guidance in the mouse spinal cord. Development *126*, 3649–3659.

Mirzayan, C. (1997). Structure-Function Analysis of the Chemoattractant Netrin-1 (UCSF).

Moore, S.W., Zhang, X., Lynch, C.D., and Sheetz, M.P. (2012). Netrin-1 attracts axons through FAK-dependent mechanotransduction. J. Neurosci. *32*, 11574–11585.

Moreno-Bravo, J.A., Puiggros, S.R., Mehlen, P., and Chédotal, A. (2019). Synergistic activity of floor plate and ventricular zone-derived netrin-1 in spinal cord commissural axon guidance. Neuron. Published online January 17, 2019. https://doi.org/10.1016/j.neuron.2018.12.024.

Okada, A., Charron, F., Morin, S., Shin, D.S., Wong, K., Fabre, P.J., Tessier-Lavigne, M., and McConnell, S.K. (2006). Boc is a receptor for sonic hedgehog in the guidance of commissural axons. Nature *444*, 369–373.

Placzek, M., Tessier-Lavigne, M., Jessell, T., and Dodd, J. (1990). Orientation of commissural axons in vitro in response to a floor plate-derived chemoattractant. Development *110*, 19–30.

Ruiz de Almodovar, C., Fabre, P.J., Knevels, E., Coulon, C., Segura, I., Haddick, P.C.G., Aerts, L., Delattin, N., Strasser, G., Oh, W.-J., et al. (2011). VEGF mediates commissural axon chemoattraction through its receptor Flk1. Neuron *70*, 966–978.

Sabatier, C., Plump, A.S., Le Ma, Brose, K., Tamada, A., Murakami, F., Lee, E.Y., and Tessier-Lavigne, M. (2004). The divergent Robo family protein rig-1/Robo3 is a negative regulator of slit responsiveness required for midline crossing by commissural axons. Cell *117*, 157–169.

Serafini, T., Kennedy, T.E., Galko, M.J., Mirzayan, C., Jessell, T.M., and Tessier-Lavigne, M. (1994). The netrins define a family of axon outgrowth-promoting proteins homologous to C. elegans UNC-6. Cell *78*, 409–424.

Serafini, T., Colamarino, S.A., Leonardo, E.D., Wang, H., Beddington, R., Skarnes, W.C., and Tessier-Lavigne, M. (1996). Netrin-1 is required for commissural axon guidance in the developing vertebrate nervous system. Cell *87*, 1001–1014.

Tessier-Lavigne, M., Placzek, M., Lumsden, A.G.S., Dodd, J., and Jessell, T.M. (1988). Chemotropic guidance of developing axons in the mammalian central nervous system. Nature *336*, 775–778.

Timofeev, K., Joly, W., Hadjieconomou, D., and Salecker, I. (2012). Localized netrins act as positional cues to control layer-specific targeting of photoreceptor axons in Drosophila. Neuron *75*, 80–93.

Varadarajan, S.G., Kong, J.H., Phan, K.D., Kao, T.-J., Panaitof, S.C., Cardin, J., Eltzschig, H., Kania, A., Novitch, B.G., and Butler, S.J. (2017). Netrin1 produced by neural progenitors, not floor plate cells, is required for axon guidance in the spinal cord. Neuron *94*, 790–799.e3.

Varadarajan, S.G., and Butler, S.J. (2017). Netrin1 establishes multiple boundaries for axon growth in the developing spinal cord. Dev. Biol. *430*, 177–187.

Wang, H., Copeland, N.G., Gilbert, D.J., Jenkins, N.A., and Tessier-Lavigne, M. (1999). Netrin-3, a mouse homolog of human NTN2L, is highly expressed in sensory ganglia and shows differential binding to netrin receptors. J. Neurosci. *19*, 4938–4947.

Watanabe, K., Tamamaki, N., Furuta, T., Ackerman, S.L., Ikenaka, K., and Ono, K. (2006). Dorsally derived netrin 1 provides an inhibitory cue and elaborates the 'waiting period' for primary sensory axons in the developing spinal cord. Development *133*, 1379–1387.

Xu, K., Wu, Z., Renier, N., Antipenko, A., Tzvetkova-Robev, D., Xu, Y., Minchenko, M., Nardi-Dei, V., Rajashankar, K.R.K.R., Himanen, J., et al. (2014). Neural migration. Structures of netrin-1 bound to two receptors provide insight into its axon guidance mechanism. Science *344*, 1275–1279.

Yam, P.T., Langlois, S.D., Morin, S., and Charron, F. (2009). Sonic hedgehog guides axons through a noncanonical, Src-family-kinase-dependent signaling pathway. Neuron *62*, 349–362.

Yam, P.T., Kent, C.B., Morin, S., Farmer, W.T., Alchini, R., Lepelletier, L., Colman, D.R., Tessier-Lavigne, M., Fournier, A.E., and Charron, F. (2012). 14-3-3 proteins regulate a cell-intrinsic switch from sonic hedgehog-mediated commissural axon attraction to repulsion after midline crossing. Neuron *76*, 735–749.

Yamauchi, K., Yamazaki, M., Abe, M., Sakimura, K., Lickert, H., Kawasaki, T., Murakami, F., and Hirata, T. (2017). Netrin-1 derived from the ventricular zone, but not the floor plate, directs hindbrain commissural axons to the ventral midline. Sci. Rep. *7*, 11992.

Yung, A.R., Nishitani, A.M., and Goodrich, L.V. (2015). Phenotypic analysis of mice completely lacking netrin 1. Development *142*, 3686–3691.

Zou, Y., Stoeckli, E., Chen, H., and Tessier-Lavigne, M. (2000). Squeezing axons out of the gray matter: a role for slit and semaphorin proteins from midline and ventral spinal cord. Cell *102*, 363–375.

STAR★METHODS

KEY RESOURCES TABLE

REAGENT or RESOURCE	SOURCE	IDENTIFIER
Antibodies		
Goat Anti-Human Robo3 Polyclonal antibody	R and D Systems	Cat# AF3076; RRID: AB_2181865
Mouse Anti-Neuronal Class III beta-Tubulin (TUJ1) Monoclonal Antibody	Covance Research Products Inc	Cat# MMS-435P; RRID: AB_2313773
Rabbit Anti-Neuronal Class III beta-Tubulin Purified Monoclonal Antibody	Covance Research Products Inc	Cat# MRB-435P-100; RRID: AB_663339
Rat Anti-Neural Cell Adhesion Molecule L1, clone 324 antibody	Millipore	Cat# MAB5272; RRID: AB_2133200
Rabbit Anti-Hb9 Antibody	Dr. Samuel L. Pfaff The Salk Institute for Biological Studies	Cat# rabbit a-Hb9 6055; RRID: AB_2715641
Mouse Anti-Isl1/2 Monoclonal Antibody	DSHB	Cat# 39.4D5; RRID: AB_2314683
Goat Anti-Rat ROBO1 Polyclonal antibody	R and D Systems	Cat# AF1749; RRID: AB_354969
Goat Anti-Contactin-2 / TAG1 Polyclonal Antibody	R and D Systems	Cat# AF4439; RRID: AB_2044647
Rat Anti-GFP Monoclonal Antibody	Nacalai Tesque	Cat# 04404-84; RRID: AB_10013361
Mouse Anti-neurofilament (NF-M) antibody	DSHB	Cat# 2H3; RRID: AB_531793
Goat Anti-Rat TrkA Polyclonal Antibody	R and D Systems	Cat# AF1056; RRID: AB_2283049
Rabbit Anti-TrkC Monoclonal Antibody	Cell Signaling Technology	Cat# 3376S; RRID: AB_2155283
Mouse anti-HNF3β monoclonal antibody	DSHB	Cat# 4C7; RRID: AB_528255
Rabbit anti-Pax6 polyclonal antibody	Biolegend	Cat#: 901301; RRID: AB_2565003
Donkey Anti-Mouse IgG (H+L) Antibody, Alexa Fluor 488 Conjugated	Thermo Fisher Scientific	Cat# A-21202; RRID: AB_141607
Donkey Anti-Mouse IgG (H+L) Antibody, Alexa Fluor 568 Conjugated	Thermo Fisher Scientific	Cat# A10037; RRID: AB_2534013
Donkey Anti-Mouse IgG (H+L) Antibody, Alexa Fluor 647 Conjugated	Thermo Fisher Scientific	Cat# A-31571; RRID: AB_162542
Donkey Anti-Rabbit IgG (H+L) Antibody, Alexa Fluor 488 Conjugated	Thermo Fisher Scientific	Cat# A-21206; RRID: AB_2535792
Donkey Anti-Rabbit IgG (H+L) Antibody, Alexa Fluor 568 Conjugated	Thermo Fisher Scientific	Cat# A10042; RRID: AB_2534017
Donkey Anti-Rabbit IgG (H+L) Antibody, Alexa Fluor 647 Conjugated	Thermo Fisher Scientific	Cat# A-31573; RRID: AB_2536183
Donkey Anti-Goat IgG (H+L) Antibody, Alexa Fluor 488 Conjugated	Thermo Fisher Scientific	Cat# A-11055; RRID: AB_2534102
Donkey Anti-Goat IgG (H+L) Antibody, Alexa Fluor 568 Conjugated	Thermo Fisher Scientific	Cat# A-11057; RRID: AB_2534104
Donkey Anti-Goat IgG (H+L) Antibody, Alexa Fluor 647 Conjugated	Thermo Fisher Scientific	Cat# A-21447; RRID: AB_2535864
Donkey Anti-Rat IgG (H+L) Antibody, Alexa Fluor 488 Conjugated	Thermo Fisher Scientific	Cat# A-21208; RRID: AB_2535794
Donkey Anti-Rat IgG (H+L) Antibody, Alexa Fluor 647 Conjugated	Jackson ImmunoResearch Labs	Cat# 712-605-153; RRID: AB_2340694
Donkey anti-rabbit IgG, Alexa Fluor 488 conjugated	Jackson ImmunoResearch Labs	Cat# 711-545-152; RRID: AB_2313584
Donkey anti-rabbit IgG, Cy3 conjugated	Jackson ImmunoResearch Labs	Cat# 711-165-152; RRID: AB_2307443
Donkey anti-goat IgG, Cy3 conjugated	Jackson ImmunoResearch Labs	Cat# 705-165-147; RRID: AB_2307351
Normal Donkey Serum	Jackson ImmunoResearch Labs	Cat# 017-000-121; RRID: AB_2337258
Chemicals, Peptides, and Recombinant Proteins		
Dichloromethane (DCM)	Sigma-Adrich	Cat# 270997 CAS Number: 75-09-2
Benzyl ether (DBE)	Sigma-Adrich	Cat# 108014 CAS Number: 103-50-4

(*Continued on next page*)

Continued

REAGENT or RESOURCE	SOURCE	IDENTIFIER
UltraPure Agarose	Invitrogen	Cat# 16500500 CAS Number: 9012-36-6
Triton X-100	Sigma-Adrich	Cat# X100-500ML CAS Number: 9002-93-1
Tween 20	Sigma-Adrich	Cat# P2287-500ML CAS Number: 9005-64-5
Poly-D-lysine hydrobromide	Sigma-Adrich	Cat# P6407-10X5MG CAS Number 27964-99-4
Recombinant Mouse Sonic Hedgehog/Shh, CF	R and D Systems	Cat# 464-SH/CF
Recombinant Mouse Netrin-1 Protein, CF	R and D Systems	Cat# 1109-N1/CF
Recombinant Human Sonic Hedgehog (C24II) N terminus	R and D Systems	Cat# 1845-SH
Poly-L-lysine solution (molecular weight 70,000-150,000, concentration: 0.01%)	Sigma-Aldrich	P4707
Hoechst 33342	Thermo Fisher Scientific	Cat# H3570; CAS Number: 23491-52-3
Experimental Models: Organisms/Strains		
Mouse: C57BL/6	The Jackson Laboratory	IMSR Cat# JAX:000664; RRID: IMSR_JAX:000664
Mouse: HB9-GFP	The Jackson Laboratory	IMSR Cat# JAX:005029; RRID: IMSR_JAX:005029
Mouse: Shh-Cre	The Jackson Laboratory	IMSR Cat# JAX:005622; RRID: IMSR_JAX:005622
Mouse: netrin1^{f1} (Ntn1^{tm1Eia})	Brunet et al., 2014	N/A
Mouse: netrin1^{f2}	Dominici et al., 2017	N/A
Mouse: BOC^{tm1Aok}		MGI Cat# 3696406; RRID: MGI:3696406
Rat: ARS/Sprague Dawley	Charles River (St. Constant, Canada)	N/A
Software and Algorithms		
AutoQuant X3 software	Media Cybernetics	http://www.mediacy.com/autoquantx3; RRID: SCR_002465
Imspector software	LaVision Biotec	https://www.lavisionbiotec.com/
Imaris x64 software (version 8.0.1)	Bitplane	http://www.bitplane.com/imaris/imaris; RRID: SCR_007370
GraphPad Prism 7	GraphPad	https://www.graphpad.com/; RRID: SCR_002798
ImageJ	NIH	https://imagej.nih.gov/ij/
Volocity 6.0	PerkinElmer	http://www.perkinelmer.com/lab-solutions/resources/docs/BRO_VolocityBrochure_PerkinElmer.pdf
Other		
Dunn Chamber	Hawksley	DC-100

CONTACT FOR REAGENT AND RESOURCE SHARING

Further information and requests for resources and reagents should be directed to and will be fulfilled by the Lead Contact, Marc Tessier-Lavigne (tessier3@stanford.edu).

EXPERIMENTAL MODEL AND SUBJECT DETAILS

Animals

All animal work was performed in accordance with: the Canadian Council on Animal Care Guidelines and approved by the IRCM Animal Care Committee (work at IRCM), or in compliance with NIH guidelines and protocols approved by the IACUC of The Rockefeller University or Stanford University (work at Rockefeller or Stanford). Staged pregnant female Sprague Dawley rats were obtained from Charles River. Mice were maintained in the IRCM specific pathogen-free animal facility. All mice were maintained on a C57BL/6 genetic background (The Jackson Laboratory). The *Shh:Cre* line (B6.Cg-Shh$^{tm1(EGFP/cre)Cjt}$/J) was obtained from The Jackson Laboratory (Harfe et al., 2004). The *Boc* mutant line (Boc^{tm1Aok}/Boc^{tm1Aok}) was kindly provided by A. Okada and S. K. McConnell (Stanford University) (Okada et al., 2006). The conditional *netrin1* lines have been previously described: *netrin*$^{f1/f1}$ (*Ntn1*^{tm1Eia}) (Brunet et al., 2014) and *netrin1*$^{f2/f2}$ (Dominici et al., 2017). Embryonic day 0 (E0) was defined as midnight of the night before a plug was found. Tissue from embryos of either sex (not determined) were used for experiments. In some embryos, the *Shh:Cre* line induced a

recombination of one of the *netrin1*$^{f2/f2}$ alleles, leading essentially to *netrin1*$^{f2/-}$ embryos, as confirmed by PCR genotyping. These *netrin1*$^{f2/-}$ embryos were phenotypically indistinguishable from *netrin1*$^{f2/f2}$ embryos and were thus pooled together for analysis.

METHOD DETAILS

Section staining and microscopy

For immunostaining of spinal cord cross-sections, mouse embryos were collected at E11.5, fixed in 4% PFA for 1 hour at 4°C or at room temperature, transferred to 10-30% sucrose in PBS at 4°C overnight, then embedded in gelatine-sucrose or OCT and frozen. 16-20 μm sections were cut. Samples were then blocked with PBS + 3% or 10% donkey serum + 0.1% Triton X-100 in PBS pH 7.4 for 1 hour at room temperature. The blocking solution was replaced with the primary antibody diluted in 1% PHT (1% heat-inactivated donkey serum, 0.1% Triton X-100 in PBS pH 7.4) and incubated overnight at 4°C. The secondary antibody was diluted in 1% PHT and incubated for 1 hour at room temperature. Probes for Netrin-1 *in situ* were generated targeting exon 2 of the mouse netrin-1 gene to validate the conditional allele removal (Brunet et al., 2014). In situ hybridization was performed as described (Marillat et al., 2002). Coverslips were mounted in Fluoromount G (Electron Microscopy Sciences) or in Mowiol (Sigma) and imaged with a Nikon Eclipse 90i fluorescent microscope with a 10X objective coupled to a Nikon QiMc camera (Nikon, Japan) or a Leica SP8 confocal microscope with 20X objective (Leica, Germany). Image stacks were deconvolved with AutoQuant X3 software (Media Cybernetics) to enhance the spatial signal allocation.

Whole embryo immunostaining and microscopy

Mouse embryos were collected at E11.5, fixed in 4% PFA at 4°C overnight. Fixed samples were washed in PBS for 1 hr three times, then subjected to the Adipo-Clear procedure (Chi et al., 2018) for whole mount immunostaining and imaging of Robo3+ commissural axons. The antibodies used here were: Robo3 (R&D Systems AF3076; 1:200), and secondary antibody conjugated with Alexa-647 was purchased from Thermo Fisher Scientific (1:200). Whole E11.5 embryos were imaged on a light-sheet microscope (Ultramicroscope II, LaVision Biotec) equipped with 4X RI-matched objective lenses and an sCMOs camera (Andor Neo) with the ImspectorPro software (LaVision BioTec). The image stacks were processed using Imaris x64 software (version 8.0.1, Bitplane) to generate surface contour using "normal shading" function based on Robo3 staining to visualize commissural axon organization in 3D, and static 3D pictures were generated using the "snapshot" tool.

Dorsal spinal cord (DSC) explant culture and outgrowth quantification on 2D substrates

8-well chambered cell culture slides were coated with 10 μg/ml PDL (Sigma P6407) at room temperature overnight, and then with varying concentrations of netrin1 (R&D 1109-N1/CF) or Shh (R&D 464-SH/CF) proteins at 37°C for 3 hours in a cell culture incubator. DSC explants were obtained from E11.5 mouse developing spinal cord as previously described (Xu et al., 2014), and cultured in growth factor-free medium [Neurobasal medium supplemented with 2% B-27, 2 mM glutamine, 100 U/ml penicillin, 100 μg/ml streptomycin, 0.5% methyl-cellulose, and 0.75% glucose] with the ventricular side facing toward the culture surface. After culture in a 5% CO_2, 95% humidity incubator at 37°C for 16 hours, explants were fixed and immunostained with Tuj antibody. Explant outgrowth was measured using the Tuj IHC signal as previously described (Xu et al., 2014).

Dissociated commissural neuron culture

Dissociated commissural neuron cultures were prepared from the dorsal fifth of E13.5 rat neural tubes as previously described and maintained at 5% CO_2 in a humidified incubator (Langlois et al., 2010; Yam et al., 2009). Each experiment was performed using cells prepared and pooled from the same litter. Neurons were plated in Neurobasal supplemented with 10% heat-inactivated FBS and GlutaMAX (Invitrogen, Burlington, ON, Canada). After ~20 h, the medium was changed to Neurobasal supplemented with 2% B27 and GlutaMAX. Dissociated commissural neurons were used for experiments 30-58 h after plating (1-2 days *in vitro*).

Dunn chamber axon guidance assay and analysis

To quantify the growth cone turning of commissural neurons in response to chemical gradients, we performed the Dunn chamber axon guidance assay as described previously (Yam et al., 2009). Briefly, commissural neurons were plated at a low density of 120,000–180,000 cells/well in six-well plates on acid-washed poly-L-lysine (100 μg/ml)-coated 18 mm square #3D coverslips (Fisher Scientific). After 1-2 DIV, coverslips were then assembled into Dunn chambers. Gradients were generated in the Dunn chamber with 150 ng/ml or 450 ng/ml netrin-1 (VI.V-Fc, Keino-Masu et al., 1996), 0.1 μg/ml recombinant human Shh (C24II, R&D Systems), or buffer containing BSA (the vehicle for Shh) in the outer well.

After Dunn chamber assembly, the behavior of commissural neurons was monitored by time-lapse phase contrast microscopy. Images were acquired for a minimum of 2 h at 37°C on a Leica DMIRE2 inverted microscope (Leica, Germany) equipped with a heated chamber and a MS-2000 XYZ automated stage (ASI, Eugene, OR) using a 10 × or 20 × Fluotar objective. All images were collected on an Orca ER CCD camera (Hamamatsu) using Volocity (Improvision, Waltham, MA).

The angle turned was defined as the angle between the original direction of the axon and a straight line connecting the base of the growth cone from the first (0 h) to the last (2 h) time point of the assay. Axons that were already growing parallel up the gradient (i.e.,

those axons with an initial orientation < 20° with respect to the gradient) were excluded from the analysis since they were already following the chemoattractant gradient.

QUANTIFICATION AND STATISTICAL ANALYSIS

Statistical analysis was performed with GraphPad Prism 7 (https://www.graphpad.com/). All error bars represent SEM and asterisks (*) indicate significance as follows: * = $p < 0.05$, ** = $p < 0.01$, *** = $p < 0.001$, n.s. = not significant ($p > 0.05$). The statistical analysis used in each experiment and the definition of n are stated in the figure legends. All t tests were two-tailed.